Are needles of *Pinus pinaster* more vulnerable to xylem embolism than branches? New insights from X-ray computed tomography

Running title: Embolism resistance of pine needles

Pauline S. Bouche[1,2,3], Sylvain Delzon[2,3], Brendan Choat[4], Eric Badel[4], Timothy J. Brodribb[5], Regis Burlett[2,3], Hervé Cochard[6], Katline Charra-Vaskou[6], Bruno Lavigne[2,3], Shan Li[1], Stefan Mayr[7], Hugh Morris[1], José M. Torres Ruiz[2,3], Vivian Zufferey[8], Steven Jansen[1]

[1]Institute for Systematic Botany and Ecology, Ulm University, D-89081, Ulm, Germany

[2]INRA, UMR1202 BIOGECO, F-33610 Cestas, France

[3]University of Bordeaux, BIOGECO, UMR 1202, F-33600 Pessac, France

[4]University of Western Sydney, Hawkesbury Institute for the Environment, Richmond, NSW 2753, Australia

[5]School of Plant Science, University of Tasmania, Hobart, Tas. 7001, Australia

[6]INRA, UMR 457 PIAF, Clermont University, F-63100 Clermont-Ferrand, France

[7]Department of Botany, University of Innsbruck, A-6020 Innsbruck, Austria

[8]Agroscope, Institut des sciences en production végétale IPV, CH-1260 Nyon, Switzerland

Corresponding author: Pauline Bouche

Tel: +33 5 40 00 38 91

Email: pauline.bouche33@gmail.com

This article has been accepted for publication and undergone full peer review but has not been through the copyediting, typesetting, pagination and proofreading process which may lead to differences between this version and the Version of Record. Please cite this article as doi: 10.1111/pce.12680

Abstract

Plants can be highly segmented organisms with an independently redundant design of organs. In the context of plant hydraulics, leaves may be less embolism resistant than stems, allowing hydraulic failure to be restricted to distal organs that can be readily replaced.

We quantified drought-induced embolism in needles and stems of *Pinus pinaster* using high resolution computed tomography (HRCT). HRCT observations of needles were compared with the rehydration kinetics method to estimate the contribution of extra-xylary pathways to declining hydraulic conductance.

HRCT images indicated that the pressure inducing 50% of embolised tracheids was similar between needle and stem xylem ($P_{50\ needle\ xylem}$ = -3.62 MPa, $P_{50\ stem\ xylem}$ = -3.88 MPa). Tracheids in both organs showed no difference in torus overlap of bordered pits. However, estimations of the pressure inducing 50% loss of hydraulic conductance at the whole needle level by the rehydration kinetics method was significantly higher ($P_{50\ needle}$ = -1.71 MPa) than $P_{50\ needle\ xylem}$ derived from HRCT.

The vulnerability segmentation hypothesis appears to be valid only when considering hydraulic failure at the entire needle level, including extra-xylary pathways. Our findings suggest that native embolism in needles is limited and highlight the importance of imaging techniques for vulnerability curves.

Key-words: embolism, high resolution X-ray computed tomography, needle, *Pinus pinaster*, stem, wall deformation, xylem

Introduction

Water transport in plants is driven by transpiration at the leaf level according to the cohesion-tension theory (Dixon & Joly 1895; Tyree & Zimmermann 2002). One major vulnerability associated with this transport mechanism is the entry of gas bubbles into the hydraulic pathway. In addition, the collapse of xylem tracheid walls has been observed in a few gymnosperms (Barnett 1976; Donaldson 2002). Both risks of transport failure are mainly due to tension of the xylem sap, which depends in part on the amount of drought stress experienced by a plant. Various methods have been applied over the last decades to quantify resistance to embolism in the vascular transport system of plants (Cochard *et al.* 2013), such as bench dehydration (Tyree *et al.* 1992; Bréda *et al*. 1993), air injection (Crombie *et al.* 1985; Sperry and Tyree 1990), and centrifuge techniques (Pockman *et al.* 1995; Alder *et al.* 1997). Embolism resistance in stem xylem is measured by constructing vulnerability curves, from which the xylem water potential corresponding to 50% loss of hydraulic conductivity (P_{50}) is generally considered as the standard reference point for comparison among both plant organs and species (Choat *et al.* 2012).

A number of techniques have been developed to measure hydraulic vulnerability curves for angiosperm leaves (Brodribb & Holbrook 2005; Scoffoni *et al.* 2011) and conifer needles (Cochard *et al.* 2004; Brodribb & Holbrook 2006; Johnson *et al.* 2009; Charra-Vaskou *et al.* 2012). P_{50} values measured for needles ($P_{50\ needles}$) of several conifer species are reported to vary from -0.5 MPa to less than -5 MPa (Woodruff *et al.* 2007; Domec *et al.* 2009; Brodribb & Cochard 2009; Johnson *et al.* 2009; Charra-Vaskou *et al*. 2012; Brodribb *et al.* 2014). In general, no partitioning of vulnerability of the xylary and extra-xylary pathways is considered in measuring P_{50} values of conifer needles. However, in order to compare vulnerability to embolism between leaves and stems within a single plant, separating xylem tissue from non-

xylary tissue could provide a useful approach to better understand xylem resistance to embolism at the whole-plant level. In other words, when comparing needles ($P_{50\ needle}$) with stems ($P_{50\ stem}$), only direct comparison is possible when $P_{50\ xylem}$ is considered across organs ($P_{50\ needle\ xylem}$ and $P_{50\ stem\ xylem}$).

The vulnerability segmentation hypothesis suggests that distal plant organs such as leaves and small stems should be more vulnerable to drought-induced xylem embolism than proximal organs, which would protect the carbon investment made in the trunk and large stems (Zimmermann 1983; Tyree & Ewers 1991). Lower resistance to embolism in leaves, which could act as a "hydraulic circuit breaker", is thought to prevent embolism and maintain a high water status in the main stem (Domec *et al.* 2009; Barigah *et al.* 2013; Bucci *et al.* 2013). However, while hydraulic failure of stem tissue is restricted to xylem tissue only, it remains unclear whether hydraulic dysfunction of leaves is due to embolism in the xylem tissue, hydraulic failure outside the xylem (extra-xylary tissue such as a multi-layer epidermis, leaf mesophyll and bundle sheath), changes in intercellular airspaces, or a combination of these factors. Furthermore, leaf hydraulic functioning is not only affected by xylem embolism, but also by leaf shrinkage (Scoffoni *et al.* 2014), turgor loss in extravascular tissue (Brodribb & Holbrook 2006; Knipfer & Steudle 2008), and potential collapse of xylem conduit walls. Based on cryo-SEM, collapse of tracheid walls in conifer needles was suggested by Cochard *et al.* (2004) in four conifer species, but was clearly limited to accessory transfusion tissue outside the xylem in *Podocarpus grayi* (Brodribb & Holbrook 2005).

The suggestion that embolism and wall collapse could be more common in needles than in stem xylem could indicate a potential difference in mechanical behaviour and anatomy. Based on earlier studies, tracheid and pit anatomical properties, especially overlap of the torus and double tracheid wall thickness to span ratio, were found to be highly related to

embolism resistance and mechanical support (Delzon *et al*. 2010; Pittermann *et al*. 2010; Bouche *et al*. 2014). Yet, tracheids in xylem tissue and extra-xylary tissue of conifer needles have been studied in detail for only few species.

The main goal of this study is to test the vulnerability segmentation hypothesis for *P. pinaster* using non-invasive embolism visualisation in xylem tissue of needles and stems. Hydraulic failure was investigated in both organs of *Pinus pinaster* using high-resolution X-ray computed tomography (HRCT). The HRCT technique has been applied to wood biology for various purposes, including non-destructive wood anatomy (Steppe *et al.* 2004; Brodersen *et al*. 2011), 3D reconstruction of the hydraulic pathway, and temporal dynamics of embolism refilling (Brodersen *et al.* 2013). HRCT is also a promising technique to construct vulnerability curves (McElrone *et al.* 2012, Cochard *et al.* 2014; Torres-Ruiz *et al.* 2014; Choat *et al*. 2015a). One advantage of the HRCT technique is that it allows us to test whether or not hydraulic dysfunction in needles of *P. pinaster* is due to embolism of leaf xylem and/or hydraulic dysfunction outside the xylem. The answer to this question plays a crucial role in fully understanding which cell types are responsible for vulnerability segmentation, and how leaves may function as a hydraulic circuit breaker. Therefore, vulnerability curves based on HRCT images were compared with the rehydration kinetics method (Brodribb & Holbrook 2003), which provides direct measurement of hydraulic conductance. An additional goal of this paper is to assess the potential occurrence of tracheid wall collapse in needles and stems of *P. pinaster* under severe drought stress. Both goals are complemented by detailed anatomical observations using light and electron microscopy.

Material and Methods

Plant material

This study was conducted at two synchrotron facilities between 2012 and 2013. All observations and measurements were carried out on *Pinus pinaster* Aiton. In October 2012, about ten seedlings from the INRA nursery, Pierroton France were transferred to the European Synchrotron Radiation Facility (ESRF, Grenoble, France). Plant material from one single adult tree was collected in a 15-year-old even-aged stand at the INRA facility in Pierroton (Bordeaux, France) in February 2013. During early morning, five fresh branches with needles were cut off the tree in air and transferred on the same day to the Diamond Light Source (DLS, UK), while the samples were bagged up in zip seal plastic bags (Table S1).

Needles from the seedlings and tree branches were kept intact on terminal stems while desiccating in a laboratory. The needles were removed from the stem just before performing the HRCT scan. To speed up the process of reaching water potentials below -5 MPa, needles were dehydrated using a warm air fan. At the DLS, the cuticle of several needles from mature trees was abraded with a razor blade. However, measurements were conducted only on intact (i.e., unabraded) needles from the same branch. A total number of 50 needles from a single tree and 28 needles from various seedlings were scanned (Table S1).

X-ray computed tomography

Needles collected and dehydrated as described above were cut in air with a razor blade. The distal end (ca. 12 to 15 cm long) was used to measure the water potential (ψ, MPa) with a pressure chamber (SAM PRECIS, Gradignan, France and PMS, Oregon, USA), while the basal end (±4 cm long) was scanned at approximately 2 cm from its basal end at the same time. Water potential measurements at the distal and basal end of a needle were similar for

fresh and dehydrated material. Petroleum jelly was applied on the cut end of the needle to avoid dehydration during the scan.

Needles were scanned using beamline I12 at the DLS and beamline ID19 at the ESRF. Depending on the synchrotron facility, scanning time varied between 1.5 minutes and 4 minutes, with 18 and 53 keV x-ray energy at the ESRF and DLS, respectively. This energy range provided an excellent contrast for plant tissue, water and gas volumes due to a good signal to noise ratio. Therefore, HRCT allowed us to easily distinguish embolised xylem conduits from water-filled ones, as well as other anatomical features. The samples were positioned 30 mm from the 2D detector and rotated in the x-ray beam. Scans included a 5 mm long segment of the needle. Raw 2D projections were then reconstructed into TIF image slices. The spatial resolution obtained varied from 1.40 µm to 1.62 µm.

Previous experiments have shown that repeated scans at the same location of stem and leaf tissue did not change the amount of embolised conduits (Choat et al., 2015b). Since repeated scans of pine needles also showed no effect on embolism formation, artefacts due to microCT scanning can be excluded.

Anatomical observations

Three scans taken from the bottom, middle and top of the needle area scanned were randomly selected for each needle to obtain anatomical data. The scan contrast allowed us to quantify the number of embolised tracheids (T_E) in xylem of the two vascular bundles as viewed in a transverse section. As the contrast of the scans was slightly lower for water-filled tracheids, we were not able to measure the total number of tracheids (T_T) for each scan. However, semi-thin (ca. 500 nm thick) sections of five needles from the same tree that was used for HRCT, and from nine needles of three seedlings, were investigated with a light microscope in order to estimate T_T (Table S1). These observations confirmed that T_T showed little or no variation

between needles and also within a given needle, varying from 186 to 191 tracheids in seedling needles (mean value = 188 ± 2), and from 255 to 261 tracheids (mean value = 258 ± 3) in adult needles. We paid special attention to selecting a branch from the tree that had a similar orientation, height, and light exposure than the branches used for HRCT. Due to quantitative differences in the anatomy of protoxylem as compared to meta-xylem, and based on the assumption that protoxylem tracheids do not contribute to water transport in mature needles (Esau 1977; Kubo *et al.* 2005), we excluded protoxylem tracheids when measuring T_T and T_E. The tracheid lumen diameter (D_T), the double tracheid wall thickness (T_W), and the thickness to span ratio ($T_W\ D_T^{-1}$) of the tracheids were measured on 500 nm thick sections using light microscopy.

The anatomical and functional properties of bordered pits in xylem of seedling and tree needles were determined based on three seedlings and the same adult tree as selected for our HRCT scans (Table S1). Stem anatomical data were based on branches (diameter < 1cm) from adult trees and retrieved from Bouche *et al.* (2014). The horizontal pit aperture diameter (D_{PA}) and torus diameter (D_{TO}) were measured using images based on scanning and transmission electron microscopy (SEM and TEM, respectively) in order to determine the torus-aperture overlap (O).

In order to quantify the potential wall deformation of xylem tracheids, eight scans were selected along a broad range of water potential (from -0.4 to -7 MPa for needles from seedlings, and from -0.6 MPa to -8.4 MPa for needles from the tree selected). The shape of the tracheids as viewed in transverse sections was quantified by the isoperimetric quotient (Q) and defined by Weinsstein *et al.* (1999) as:

$$Q = 4\ \pi\ A\ P^{-2}$$

, where A is the lumen area and P the wall perimeter.

The pressure required to induce wall implosion (P_{WI}) was estimated according to Domec *et al.* (2006):

$$P_{WI} = (\omega/\beta)(T_W/D_T)^2 L_E (I_H/I_S)$$

, where ω was the strength of the wall material assumed to be 80 MPa (Hacke *et al.* 2001), and β was a coefficient taken as 0.25. The moment ratio (I_H/I_S) represented the ratio of the second moment of area of a wall with pit chamber (I_H) to that of a solid wall with no pit chamber present (I_S). Hacke *et al.* (2004) showed that I_H/I_S did not change with air-seeding pressure, and was on average ~0.95 in conifers. The ligament efficiency [$L_E = 1 - D_{PA} / (D_{PM} + L_{PB})$] quantified the spatial distribution of the pit aperture in the wall, and L_{PB} represented the distance between neighbouring pit borders.

Xylem anatomical measurements were conducted without checking a priori the corresponding water potential values to guarantee objectivity for T_E measurements. For light microscopy, SEM and TEM, a minimum of 25 measurements were collected for each anatomical trait (T_T, D_T, T_W, D_{PA}, D_{TO}, O and L_{PB}) based on a total of 11 fresh needles from the same tree that was used for HRCT, and on 12 fresh needles from three 2-year-old seedlings from the Planfor nursery, Mont de Marsan, France (Table S1).

In addition, three scans (from the top, middle and bottom of the area scanned) of both tree and seedling needles were selected to measure the percentage loss of tissue area (*PLA*, %) by dehydration. $PLA = A_i/A_f \times 100$

, where A_i and A_f were areas measured for each tissue separately and for the whole needle at $P_{initial}$ and P_{final}, respectively. $P_{initial}$ was -0.4 and -0.1 MPa, while P_{final} was -8.4 and -7 MPa for the tree and seedling needles selected, respectively.

All anatomical measurements were conducted using ImageJ software (Rasband 1997-2014).

Electron microscopy

Standard protocols were used to prepare needle samples from the same single tree and seedlings, from the same growing location, for SEM and TEM. For SEM, needles were cut with a fresh razor blade in order to have the radial tracheid walls exposed. After drying for 24 hours in an oven at 60°C, the samples were fixed on stubs, coated with gold using a sputter coater (108 Auto, Cressington, UK) for 40s at 20mA, and observed under 5 kV with a benchtop SEM (PhenomG2 pro, FEI, The Netherlands).

TEM was done with fresh material that was first washed several times with a phosphate-buffer saline solution and fixated in 2% aqueous osmium tetroxide solution, then dehydrated through a gradual ethanol series (30%, 50%, 70%, 90%), and embedded in resin (Epon). Semi-thin sections were cut with an ultramicrotome (Leica Ultracut UCT, Leica Microsystems, Vienna, Austria), stained with 0.5% toluidine blue in 0.1 M phosphate buffer and mounted on microscope slides using Eukitt. Ultra-thin sections between 60 nm and 100 nm were mounted on copper grids (Athena, Plano GnbH, Wetzlar, Germany) and observed with a JEM-1210 TEM (Jeol, Tokyo, Japan) at 80 kV. Digital images were taken using a MegaView III camera (Soft Imaging System, Münster, Germany).

Vulnerability curves based on HRCT and rehydration kinetics technique

Vulnerability curves based on HRCT images were reconstructed for the tree and seedling needles (n = 50 and 28, respectively), covering a water potential that ranged from – 0.1 MPa to -8.4 MPa. Measurements were conducted on three transverse sections for each scan, i.e. at the top, in the middle, and near the top of each needle volume scanned in order to include axial variation in embolism within the volume scanned. Vulnerability curves were obtained by plotting the percentage of embolised tracheids versus xylem water potential (MPa) following the equation:

$$\text{Percentage of embolised tracheids} = 100\left(1 - \frac{FT_i}{FT_{max}}\right)$$

, where $F_T = T_T - T_E$ measured at each water potential. Curves were fitted using the following equation (Pammenter & Vander Willigen 1998):

$$\text{Percentage of embolised tracheids} = \frac{100}{\left[1+exp\left(\frac{S}{25}x\left(\Psi - P_{50\ xylem}\right)\right)\right]}$$

, where $P_{50\ xylem}$ (MPa) is the xylem pressure inducing 50% of embolised tracheids, and S (% MPa^{-1}) is the slope of the vulnerability curve at the inflexion point.

Data from Choat et al. (2015b) were retrieved to produce a stem vulnerability curve based on HRCT images. A total of 22 two-year-old seedling stems of *P. pinaster* were analysed at the Swiss Light Source (SLS, Switzerland, Table S1), covering a water potential that ranged from -0.25 MPa to -8 MPa. Stem water potentials were measured just before the scans, by using a Scholander Pressure Chamber. Prior to water potential measurements, needles were covered with plastic bags and aluminium foil for at least 30 min. Similar to needle vulnerability curves, the stem vulnerability curve based on HRCT was obtained by plotting the percentage of embolised tracheids versus xylem water potential (MPa).

In addition, the rehydration kinetics method was used to obtain a needle vulnerability curve. In June 2014, 15 branches from the same tree that was used for the DLS scans were cut early in the morning when ψ was high and then allowed to desiccate for one week. Branches were bagged for 1 hour to ensure closure of stomata and homogeneity of leaf water potential. Two needles were then removed to determine the water potential, and the terminal part of a stem with similar leaf area was cut and connected to a flow meter to measure hydraulic conductance under rehydration according to Brodribb & Cochard (2009). To avoid possible obstruction of the water flow into the needle due to resin, the stem was debarked prior to conducting a measurement. The possibility of fast and slow tissue compartments was tested

by monitoring leaf water potential continuously after rehydration. This approach allowed us to observe whether water potential drifted slowly to a different steady state due to weakly connected needle tissue, with for instance fast rehydration of the xylem, followed by slow flow into transfusion tracheids or outer mesophyll cells. Since our kinetic data showed that the needles behaved as a uniform capacitor with constant, asymptotic rehydration, the hydraulic conductance of a needle as measured with the rehydration technique is likely to encompass the entire needle structure, including xylem and non-xylem tissue. This means that the loss of hydraulic conductance measured using the rehydration technique may not be due to embolism in xylem tracheids only, but could also be caused by the loss of hydraulic conductance in extra-xylary tissue and intercellular spaces.

Statistical analyses

Variation of anatomical traits between organs (tree needles and tree stems retrieved from Bouche *et al.,* 2014) and within a single organ (needles from one tree and seedlings) were assessed using one-way analyses of variance (ANOVAs). Data and statistical analyses were conducted using SAS software (version 9.4 SAS Institute, Cary, NC, USA).

Results

Vulnerability curves of needles and stems

HRCT images allowed clear observation of embolism in xylem tracheids of *P. pinaster* needles with increasing drought stress (Fig. 1). The first tracheids that embolised were located near the protoxylem (Fig. 1a, b), and embolism spread further in a radial direction towards the phloem tissue (Fig. 1c, d, e, f). Comparison of microCT slices from the top, centre, and bottom of the HRCT area that was scanned did not show any major difference

with respect to the amount and spatial distribution of embolised tracheids. Contrary to xylem tracheids, embolism was not observed in transfusion tracheids, but intercellular spaces between the branched mesophyll cells enlarged and became more air-filled under increasing drought stress (Fig. 2).

HRCT showed similar P_{50} values for needle xylem ($P_{50\ needle\ xylem}$ = -3.56 MPa and -3.62 for seedling and tree needles, respectively, Fig. 3a) and stem xylem ($P_{50\ stem\ xylem}$ = -3.88 MPa, Fig 3b). However, the starting point of the vulnerability curve differed between needles (PLC = 20%) and stems (PLC = 8%), even though non-functional tracheids could be observed in HRCT scans of both organs at a water potential close to 0 MPa (Fig. 1a, b).

The rehydration technique indicated a 50% loss of the hydraulic conductance of the whole needle ($P_{50\ needle}$) at -1.71 MPa (Fig 3c). Moreover, the latter method showed a loss of 90% of the hydraulic conductance of the whole needle ($P_{90\ needle}$) at around -3.6 MPa, which was close to the $P_{50\ xylem}$ values estimated for stem and tree needle xylem.

Xylem anatomy

The tracheid lumen diameter (D_T) was significantly higher in xylem from stems than needles. Moreover, the thickness to span ratio of needle tracheids ($T_W\ D_T^{-1}$) was lower than stem tracheids ($T_W\ D_T^{-1}$ = 0.15 and 0.22, respectively, Table 1). This difference in $T_W\ D_T^{-1}$ was mainly due to variation in the double tracheid wall thickness (T_W), which was 1.6 times lower in needles than in stems (T_W = 2.52 ± 0.1 µm and 4.16 ± 0.15 µm, respectively, Table 1).

The pit membrane diameter was larger in stems than in needles, and the pit aperture (D_{PA}) and torus diameter (D_{TO}) were also wider (D_{PA} = 3.24 ± 0.06 µm and 1.97 ± 0.2 µm; D_{TO} = 6.40 ± 0.06 µm and 4.18 ± 0.15 µm, respectively; Table 1). Nevertheless, these quantitative differences in pit structure did not affect the value of the torus-aperture overlap (O = 0.52 ± 0.02 and 0.49 ± 0.02 for branches and needles, respectively, Table 1).

Significant differences were also found when comparing tracheids in tree needles with seedling needles. The thickness to span ratio ($T_W\ D_T^{-1}$) was lower in the seedlings than in the tree needles ($T_W\ D_T^{-1}$ = 0.13 ± 0.01 and 0.16 ± 0.01, respectively, Table 1). The pressure corresponding to tracheid wall collapse ($P_{Wí}$) showed values of -7 MPa and -3.89 MPa for tree needles and seedling needles, respectively, and was most negative (-10.5 MPa) for stems. No significant differences were found in the bordered pit anatomy of tracheids between tree needles and those of seedlings.

Needle and xylem wall deformation

HRCT images did not show tracheid wall deformation in stem xylem, but minor differences were found between tree needles and seedling needles. Needles from the tree conserved their more or less regular tracheid shape even at the most negative water potential measured (Q = 0.87 ± 0.01 at ψ = -0.4MPa and Q = 0.86 ± 0.01 at ψ = -8.4 MPa, Fig. 2a, c, e, g, 4). However, the shape of the entire needle changed considerably during dehydration. The adaxial side of the needle, which was straight when fully hydrated, became V-shaped at more negative water potentials (Fig.2g, 5). At -8.4 MPa, the tree needle reduced its total area by 23%, with a 15.4% reduction of the mesophyll area, and a 46.9% shrinking of the transfusion tissue area. The vascular bundles and multi-layered epidermis (epidermis + hypodermis), however, showed little difference in tissue area between a hydrated and dehydrated needle (Table 2, Fig. 5). The limited resolution of the HRCT scans did not allow us to accurately quantify the increase in air space between mesophyll cells during dehydration.

The shape of the seedling needles showed a stronger deformation than the tree needles as not only the adaxial side became curved, but also the abaxial side showed an irregular, folded pattern (Fig. 2b, d, f, h). Upon dehydration, the entire seedling needle lost 68.9 % of its total area mainly due to shrinkage of transfusion tissue and mesophyll (ψ = - 7 MPa; PLA = 46.9

% and 74.3%, respectively, Table 2; Fig 5c, d, S1, S2). Unlike tree needles, the epidermis and vascular bundles of seedling needles also showed relatively high shrinkage (PLA = 36.5 and 28.1%, respectively; Table 2; Fig 5c, d, S1, S2). The seedling needles did not show xylem wall deformation at the highest water potential measured (i.e., -0.58 MPa, Q = 0.9 ± 0.01, Fig. 2b, 4), but tracheid wall deformation was first observed at -2 MPa (Q = 0.78 ± 0.02, Fig. 1d, 4), and was likely to occur at the most negative water potential measured (i.e., -7 MPa, Q = 0.67 ± 0.02, Fig. 1f, 4).

Discussion

Vulnerability curves based on the centrifuge, rehydration kinetics and acoustic emissions show that the loss of hydraulic conductance in needles occurs at a higher water potential than in stems (Charra-Vaskou *et al.* 2012; Domec *et al.* 2009; Johnson *et al.* 2011; Johnson *et al.* 2012). Yet, one of our major results is that needle xylem was not more vulnerable to embolism than stem xylem. This finding suggests that the drought-induced decline of hydraulic conductance of *P. pinaster* needles was not due to xylem embolism but rather to hydraulic dysfunction of extra-xylary tissue in the needle. Therefore, the vulnerability segmentation hypothesis does not apply to *P. pinaster* when considering the xylem tissue in stems and needles exclusively, and is valid only at the stem vs whole-needle level (including xylary and extra-xylary pathways in needles). The partitioning of vulnerability of xylary and extra-xylary tissue provides a novel view on earlier tests of the vulnerability segmentation hypothesis that were based on whole-leaf vulnerability approaches (Tyree & Ewers 1991; Tyree & Zimmermann 2002; Tsuda & Tyree 1997).

As we did not observe any embolism in transfusion tracheids (Fig. 5, S1, S2), but considerable changes in the intercellular airspaces of the armed mesophyll cells of *P. pinaster*

(Fig. 5), our observations suggest that the bulk of leaf hydraulic conductance decline under drought stress may not have been caused by embolism but by changes in the extra-xylary pathways. Indeed, the extra-xylary pathways (including transfusion and mesophyll tissue) of tree and seedling needles appeared to lose 30 % and 70 % of their initial surface area, respectively. As such, it is possible that folding of the transfusion tracheid walls (see below; Fig. S1, S2) in combination with closing off of intercellular pathways in the leaf mesophyll acted as a major defence mechanism against dehydration of the xylem. This suggestion is in agreement with Scoffoni *et al*. (2014), who showed based on computer simulations of the leaf hydraulic system that xylem water potentials in leaves may rarely reach pressures that induce air-seeding and embolism.

The similar xylem embolism resistance between stems and needles was supported by the bordered pit anatomy of tracheids. In particular, given that embolism resistance in conifers is strongly associated with torus overlap of bordered pit apertures (Delzon *et al*. 2010; Pittermann *et al.* 2010; Bouche *et al.* 2014), similar values of torus-aperture overlap for needles and branches suggest that the xylem tissue of both organs was equally vulnerable to embolism. Whether or not the vulnerability segmentation hypothesis can be supported for a wide range of conifers and angiosperms cannot be generalised based on our findings and requires further research on more species.

Vulnerability curves of needles depend strongly on the method applied, and particularly on whether or not hydraulic conductance is measured at the whole needle level or limited to xylem tracheids only. Comparison of microCT with the rehydration technique illustrates that maritime pine needles had a $P_{50\ \text{needle xylem}}$ value that was twice as negative as the $P_{50\ \text{needle}}$. The fact that we did not find evidence for a water potential drift after rehydration suggests that the main hydraulic pathways of the needle were being rehydrated, and hence that the

conductance measured with the rehydration technique represents the whole needle, including extra-xylary tissue.

An alternative possibility could be that the number of embolised tracheids based on HRCT scans did not fully correspond to the specific loss of hydraulic conductance measured with the rehydration kinetics method. In theory, even when 50% of the xylem tracheids remain functional (based on HRCT images), the three-dimensional pattern of embolised tracheids could block water transport completely, resulting in 100% loss of conductance based on hydraulic measurements. However, the mainly radial patterns of embolism spreading along the few rows of xylem tracheids in needles and the rather homogeneous arrangement of similar-sized tracheids indicate that this explanation is unlikely.

Although it seems that stems and needles always have some embolised tracheids in their xylem, even at water potentials close to zero, the higher amount of embolised tracheids in needles could be caused by a difference in seasonal minimum water potential between both organs and a gradient of decreasing pressure from the roots to the needles (Tyree & Zimmermann 2002). Xylem tracheids in needles of *P. pinaster*, which have a life span of three to five years (Mediavilla *et al.* 2014), may experience a seasonal minimum water potential of -2 MPa (Delzon *et al.* 2004). The relatively high resistance to embolism in xylem of needles reported in this study suggests that high levels of embolised tracheids may not be very common under natural conditions and raises questions about daily refilling of embolised tracheids in the xylem tissue (Johnson *et al.* 2012; Choat *et al.* 2015a). Contrary to needles, the xylem tracheids in stems may be subject to less negative water potentials on a seasonal basis because of the pressure gradient at the whole plant level.

We observed a general shrinkage of needles upon dehydration. However, deformation of tracheid walls seemed to occur mainly in needles of seedlings at highly negative water

potentials, but was not observed in trees. The lower thickness to span ratio of tracheid walls in seedlings than trees could explain why the deformation of the tracheid walls was only observed in seedlings, while tracheids in tree needles were more resistant to wall deformation. Evidence of tracheid wall implosion in branch xylem of some Pinaceae has been observed in tracheids that show an extremely weak degree of lignification of their secondary wall (Barnett 1976; Donaldson 2002). However, higher lignin content in needles from early growth stages of *P. pinaster* than adult trees (Mediavilla *et al.* 2014) seems to suggest that the difference in thickness to span ratio ($T_W D_T^{-1}$) and not lignin concentration explains our findings. Bouche *et al*. (2014) showed that the seasonal minimum water potential measured in conifer species is generally less negative than the pressure needed to cause wall implosion in lignified tracheids. This suggests that xylem collapse is unlikely to occur under field conditions, contrary to Cochard *et al.* (2004). A recent study of Zhang *et al.* (2014) on *Taxus baccata* also discards wall implosion in xylem tracheids, and supports our findings by highlighting wall folding in transfusion tracheids (Fig. S1, S2; Brodribb & Holbrook 2005). As mentioned above, the seasonal minimum water potential of *P. pinaster* in the field was significantly higher than the theoretical pressure inducing tracheid wall collapse (Ψ_{min} = -2MPa; P_{WI} = -7MPa). Wall pressure implosion of seedling needles is more likely, but still more negative than the Ψ_{min} and the P_{50} values, which suggests that wall implosion of xylem tracheids in seedling needles is also uncommon in nature.

In conclusion, this study provides evidence that P_{50} values of xylem tracheids in needles of *P. pinaster* are similar to stem xylem tracheids, which is supported by anatomical evidence. This finding means that the vulnerability segmentation hypothesis only holds true for *P. pinaster* when hydraulic conductance is considered at the whole leaf level. How exactly leaf hydraulic conductance in the extra-xylary tissue declines with increasing drought stress requires more detailed anatomical observations of changes in the symplastic and/or apoplastic pathways of

transfusion tracheids, mesophyll cells and intercellular airspaces (Buckley 2014; Rockwell *et al*. 2014; Scoffoni 2014; Buckley et al. 2015).

Acknowledgments

We thank the Diamond Light Source (DLS, UK) for access to beamline I12 (proposal number 8244) and acknowledge Dr. Robert Atwood and Bob Humphreys for technical support at the DLS. Additional experiments were performed at the European Synchrotron Radiation Facility (ESRF, proposal number EC-1026, Grenoble, France) with technical support provided by Dr. Alexander Rack at the ID19 beamline. We thank the Experimental Unit of Pierroton (UE 0570, INRA, 69 route d'Arcachon, 33612 CESTAS, France) for providing plant material. The Electron Microscopy Section at Ulm University is acknowledged for the preparation of TEM samples. Andrew McElrone (UC Davis, USDA) is acknowledged for providing us with technical details to build the HRCT plant holder for scanning seedlings. This study was supported by mobility grants from the Franco-German University (UFA). Shan Li acknowledges financial support from the China Scholarship Council (CSC).

References

Alder N.N., Pockman W.T., Sperry J.S. & Nuismer S. (1997) Use of centrifugal force in the study of xylem cavitation. *Journal of Experimental Botany* **48,** 665-674.

Barigah T.S., Bonhomme M., Lopez D., Traore A., Douris M., Venisse J.S., Cochard H & Badel E. (2013) Modulation of bud survival in *Populus nigra* sprouts in response to water stress-induced embolism. *Tree Physiology* **33,** 261-274.

Barnett J.R. (1976) Rings of collapsed cells in *Pinus radiata* stemwood from lysimeter-grown trees subjected to drought. *New Zealand Journal of Forestry Science* **6,** 461-465.

Bouche P.S., Larter M., Domec J-C., Burlett R., Gasson P., Jansen S. & Delzon S. (2014) A broad survey of hydraulic and mechanical safety in the xylem of conifers. *Journal of Experimental Botany* **65,** 4419-4431.

Bréda N., Cochard H., Dreyer E. & Granier A. (1993) Field comparison of transpiration, stomatal conductance and vulnerability to cavitation of *Quercus petraea* and *Quercus robur* under water stress. *Annales des Sciences Forestières* **50,** 571-582.

Brodersen C. R., Lee E. F., Choat B., Jansen S., Phillips R. J., Shackel K. A,…, Matthews M. A. (2011) Automated analysis of three- dimensional xylem networks using high- resolution computed tomography. *New Phytologist* **191**, 1168-1179.

Brodersen C.R., McElrone A.J., Choat B., Lee E.F., Shackel K.A. & Matthews M.A. (2013) In vivo visualizations of drought-induced embolism spread in *Vitis vinifera*. *Plant Physiology* **161,** 1820-1829.

Brodribb T.J. & Cochard H. (2009) Hydraulic failure defines the recovery and point of death in water-stressed conifers. *Plant Physiology* **149,** 575-584.

Brodribb T. J. & Holbrook N. M. (2003) Stomatal closure during leaf dehydration, correlation with other leaf physiological traits. *Plant Physiology* **132**, 2166-2173.

Brodribb T.J. & Holbrook M.N. (2005) Water stress deforms tracheids peripheral to the leaf vein of a tropical conifer. *Plant Physiology* **137,** 1139-1146.

Brodribb T.J. & Holbrook N.M. (2006) Declining hydraulic efficiency as transpiring leaves desiccate: two types of response. *Plant, Cell & Environment* **29,** 2205-2215.

Brodribb T.J., McAdam S.A.M., Jordan G.J. & Martins S.C.V. (2014) Conifer species adapt to low-rainfall climates by following one of two divergent pathways. *Proceedings of the National Academy of Sciences of the United States of America*: **111,** 14489-14493.

Bucci S.J., Scholz F.G., Campanello P.I., Montti L., Jimenez-Castillo M., Rockwell F.A., …, Goldstein G. (2012) Hydraulic differences along the water transport system of South American *Nothofagus* species: do leaves protect the stem functionality? *Tree Physiology* **32**, 880-893.

Bucci S.J., Scholz F.G., Peschiutta M.L., Arias N.S. & Meinzer F.C., Goldstein G. (2013) The stem xylem of Patagonian shrubs operates far from the point of catastrophic dysfunction and is additionally protected from drought-induced embolism by leaves and roots. *Plant, Cell and Environment* **36,** 2163-2174.

Buckley T.N. (2014) The contributions of apoplastic, symplastic and gas phase pathways for water transport outside the bundle sheath in leaves. *Plant, Cell & Environment* **38,** 7-22.

Buckley T.N., John G.P., Scoffoni C. & Sack L. (2015) How does leaf anatomy influence water transport outside the xylem? *Plant Physiology* **168,** 1616-1635.

Charra-Vaskou K., Badel E., Burlett R., Cochard H., Delzon S. & Mayr S. (2012) Hydraulic efficiency and safety of vascular and non-vascular components in *Pinus pinaster* leaves. *Tree Physiology* **32,** 1161-1170.

Chave J., Coomes D., Jansen S., Lewis S.L., Swenson N.G. & Zanne A.E. (2009) Towards a worldwide wood economics spectrum. *Ecology letters* **12,** 351-366.

Choat B., Brodersen C.R. & McElrone A.J. (2015a) Synchrotron X-ray microtomography of xylem embolism in *Sequoia sempervirens* saplings during cycles of drought and recovery. *New Phytologist* **205,** 1095-1105.

Choat B., Badel E., Burlett R., Delzon S., Cochard H. & Jansen S. (2015b) Non-invasive measurement of vulnerability to drought induced embolism by X-ray microtomography. *Plant Physiology.* In press

Choat B., Jansen S., Brodribb T.J., Cochard H., Delzon S., Bhaskar R., …, Zanne A.E. (2012) Global convergence in the vulnerability of forests to drought. *Nature* **491,** 752-755.

Cochard H., Badel E., Herbette S., Delzon S., Choat B. & Jansen S. (2013) Methods for measuring plant vulnerability to cavitation: a critical review. *Journal of Experimental Botany* **64,** 4779-4791.

Cochard H., Delzon S. & Badel E. (2014) X-ray microtomography (micro-CT): a reference technology for high-resolution quantification of xylem embolism in trees. *Plant, Cell & Environment* **38,** 201-206.

Cochard H., Froux F., Mayr S. & Coutand C. (2004) Xylem wall collapse in water-stressed pine needles. *Plant Physiology* **134,** 401-408.

Crombie D.S., Hipkins M.F. & Milburn J.A. (1985) Gas penetration of pit membranes in the xylem of *Rhododendron* as the cause of acoustically detectable sap cavitation. *Australian Journal of Plant Physiology* **12,** 445-53.

Delzon S., Douthe C., Sala A. & Cochard H. (2010) Mechanism of water-stress induced cavitation in conifers: bordered pit structure and function support the hypothesis of seal capillary-seeding. *Plant, Cell & Environment* **33,** 2101-2111.

Delzon S., Sartore M. & Burlett R. (2004) Hydraulic responses to height growth in maritime pine trees. *Plant, Cell & Environment* **27,** 1077-1087.

Dixon H.H. & Joly J. (1895) On the Ascent of Sap. *Philosophical Transactions of the Royal Society B: Biological Sciences* **186,** 563-576.

Domec J-C., Lachenbruch B. & Meinzer F.C. (2006) Bordered pit structure and function determine spatial patterns of air-seeding thresholds in xylem of Douglas-fir (*Pseudotsuga menziesii*; Pinaceae) trees. *American Journal of Botany* **93,** 1588-1600.

Domec J-C., Warren J., Meinzer F. & Lachenbruch B. (2009) Safety factors for xylem failure by implosion and air-seeding within roots, trunks and branches of young and old conifer trees. *International Asoociation of Wood Anatomists* **30,** 100-120.

Donaldson L.A. (2002) Abnormal lignin distribution in wood from severely drought stressed *Pinus radiata* trees. *International Asoociation of Wood Anatomists* **23,** 161-178.

Esau K. 1977. *Anatomy of seed plants*, 2nd ed. Wiley, New York.

Espino S. & Schenk. (2009) Hydraulically integrated or modular? Comparing whole-plant-level hydraulic systems between two desert shrub species with different growth forms. *New Phytologist* **183,** 142-152.

Hacke U.G., Sperry J.S. & Pittermann J. (2004) Analysis of circular bordered pit function II. Gymnosperm tracheids with torus-margo pit membranes. *American Journal of Botany* **91,** 386-400.

Hacke U.G., Sperry J.S., Pockman W.T., Davis S.D. & McCulloh K.A. (2001) Trends in wood density and structure are linked to prevention of xylem implosion by negative pressure. *Oecologia* **126,** 457-461.

Jansen S., Schuldt B. & Choat B. (2015) Current controversies and challenges in applying plant hydraulic techniques. *New Phytologist* **205,** 961-964.

Johnson D.M., McCulloh K.A., Meinzer F.C., Woodruff D.R. & Eissenstat D.M. (2011) Hydraulic patterns and safety margins, from stem to stomata, in three eastern US tree species. *Tree Physiology* **31,** 659-668.

Johnson D.M., McCulloh K.A., Woodruff D.R. & Meinzer F.C. (2012) Hydraulic safety margins and embolism reversal in stems and leaves: why are conifers and angiosperms so different? *Plant Science* **195,** 48-53.

Johnson D.M., Woodruff D.R., McCulloh K.A. & Meinzer F.C. (2009) Leaf hydraulic conductance, measured in situ, declines and recovers daily: leaf hydraulics, water potential and stomatal conductance in four temperate and three tropical tree species. *Tree Physiology* **29,** 879-887.

Knipfer T. & Steudle E. (2008) Root hydraulic conductivity measured by pressure clamp is substantially affected by internal unstirred layers. *Journal of Experimental Botany* **59,** 2071-2084.

Kubo M., Udagawa M., Nishikubo N., Horiguchi G., Yamaguchi M., Ito J., Mimura T. Fukuda H. & Demura T. (2005) Transcription switches for protoxylem and metaxylem vessel formation. *Genes & Development* **19,** 1855-1860.

Maton C. & Gartner B.L. (2005) Do gymnosperm needles pull water through the xylem produced in the same year as the needle? *American Journal of Botany* **92,** 123-131.

McElrone A.J., Brodersen C., Alsina M., Drayton W., Matthews M., Shackel K., Wada H., Zufferey V., Choat B. (2012) Centrifuge technique consistently overestimates vulnerability to water stress-induced cavitation in grapevines as confirmed with high-resolution computed tomography. *New Phytologist* **196,** 661-665.

McElrone A.J., Choat B., Parkinson D.Y., MacDowell A. & Brodersen C.R. (2013) Using high resolution computed tomography to visualize the three dimensional structure and function of plant vasculature. *Journal of Visualized Experiments* **74.**

Mediavilla S., Herranz M., Gonzales-Zurdo P. & Escudero A. (2014) Ontogenetic transition in leaf traits: a new cost associated with the increase in leaf longevity. *Journal of Plant Ecology* **7,** 567-575.

Pammenter N. & Vander Willigen C. (1998) A mathematical and statistical analysis of the curves illustrating vulnerability of xylem to cavitation. *Tree Physiology* **18,** 589-593.

Pittermann J., Choat B., Jansen S., Stuart S.A., Lynn L. & Dawson T.E. (2010) The relationships between xylem safety and hydraulic efficiency in the Cupressaceae: the evolution of pit membrane form and function. *Plant Physiology* **153,** 1919-1931.

Pockman W.T., Sperry J.S. & O'Leary J.W. (1995) Sustained and significant negative water pressure in xylem. *Nature* **378,** 715-716.

Rockwell F.E., Holbrook M.N. & Stroock A.D. (2014) The competition between liquid and vapor transport in transpiring leaves. *Plant Physiology* **164,** 1741-1758.

Schenk H. J., Espino S. Goedhart C.M., Nordenstahl M., Martinez-Cabrera H.I. & Jones S.C. (2008) Hydraulic integration and shrub growth form linked across continental aridity gradients. *Proceedings of the National Academy of Sciences* **105,** 11248-11253.

Scholz A., Klepsch M., Karimi Z. & Jansen S. (2013) How to quantify conduits in wood? *Frontiers in plant science* **4,** 56.

Scoffoni C. (2014) Modelling the outside-xylem hydraulic conductance: towards a new understanding of leaf water relations. *Plant, Cell & Environment* **38,** 4-6.

Scoffoni C., Rawls M., McKown A., Cochard H. & Sack L. (2011) Decline of leaf hydraulic conductance with dehydration: relationship to leaf size and venation architecture. *Plant Physiology* **156,** 832-843.

Scoffoni C., Vuong C., Diep S., Cochard H. & Sack L. (2014) Leaf shrinkage with dehydration: coordination with hydraulic vulnerability and drought tolerance. *Plant Physiology* **164,** 1772-1788.

Sperry J.S. & Tyree M.T. (1990) Water-stress-induced xylem embolism in three species of conifers. *Plant, Cell & Environment* **13,** 427-436.

Spicer R. (2014) Symplasmic networks in secondary vascular tissues: parenchyma distribution and activity supporting long-distance transport. *Journal of Experimental Botany* **65,** 1829-1848.

Steppe K., Cnudde V., Girard C., Lemeur R., Cnudde J-P. & Jacobs P. (2004) Use of X-ray computed microtomography for non-invasive determination of wood anatomical characteristics. *Journal of Structural Biology* **148,** 11-21.

Torres-Ruiz J.M., Cochard H., Mayr S., Beikircher B., Diaz-Espejo A., Rodriguez-Dominguez C.M., Badel E. & Fernández J.E. (2014) Vulnerability to cavitation in *Olea europaea* current-year shoots: further evidence of an open-vessel artifact associated with centrifuge and air-injection techniques. *Physiologia Plantarum* **152,** 465-474.

Tsuda M. & Tyree M.T. (1997) Whole-plant hydraulic resistance and vulnerability segmentation in Acer saccharinum. *Tree Physiology* **17,** 351-357.

Tyree M. & Ewers F. (1991) The hydraulic architecture of trees and other woody plants. *New Phytologist* **119,** 345-360.

Tyree MT., Alexander J. & Machado J.L. (1992) Loss of hydraulic conductivity due to water stress in intact juveniles of Q*uercus rubra* and *Populus deltoides*. *Tree Physiology* **10,** 411-415.

Tyree M. & Zimmermann M. (2002) *Xylem structure and the ascent of sap.* Berlin, Germany: Springer-Verlag.

Weisstein E.W. (1999) CRC Concise Encyclopedia of Mathematics. CRC Press, Boca Raton, FL.

Woodruff D.R., McCulloh K.A., Warren J.M., Meinzer F.C. & Lachenbruch B. (2007) Impacts of tree height on leaf hydraulic architecture and stomatal control in Douglas-fir. *Plant, Cell & Environment* **30,** 559-569.

Zhang Y-J., Rockwell F.E., Wheeler J.K., Holbrook N.M. (2014) Reversible deformation of transfusion tracheids in *Taxus baccata* is associated with a reversible decrease in leaf hydraulic conductance. *Plant Physiology* **165,** 1557-1565.

Zimmermann M. (1983) *Xylem structure and the ascent of sap.* Berlin, Germany: Springer-Verlag.

Zufferey V., Cochard H., Ameglio T., Spring J-L. & Viret O. (2011) Diurnal cycles of embolism formation and repair in petioles of grapevine (*Vitis vinifera* cv. *chasselas*). *Journal of Experimental Botany* **62,** 3885-3894.

Table 1. Variation in anatomical and functional properties between tracheids from needle and stem xylem of *Pinus pinaster*. Needles were studied from seedlings and a single tree. Mean values (±SE) of the tracheid lumen diameter (D_T; µm), double tracheid wall thickness (T_W; µm), thickness to span ratio ($T_W\ D_T^{-1}$), horizontal pit aperture diameter (D_{PA}; µm), torus diameter (D_{TO}; µm) and torus-aperture overlap (O) are given for both stems and needles. The pressure inducing tracheid wall collapse is determined as P_{WI} (MPa). Bold letters (**a**, **b**, **c**) indicate when anatomical features are significantly different between stem and needles ($p<0.05$). Data of tree stems were retrieved from Bouche *et al*. (2014).

Organ	D_T	T_W	D_{PA}	D_{TO}	$T_W\ D_C^{-1}$	O	P_{WI}
Needle (tree)	16.29 ± 0.4**b**	2.52 ± 0.1**b**	1.97 ± 0.2**a**	4.18 ± 0.15**a**	0.16 ± 0.007**a**	0.52 ± 0.02**a**	-7.00
Needle (seedling)	10.65 ± 0.23**a**	1.42 ± 0.05**a**	2.58 ± 0.2**a**	5.45 ± 0.23**a**	0.13 ± 0.01**b**	0.59 ± 0.04**a**	-3.89
Stem (tree)	18.65 ± 0.43**c**	4.16 ±0.15**c**	3.24 ±0.06**b**	6.40 ± 0.06**b**	0.22 ±0.008**c**	0.49± 0.02**a**	-10.5

Table 2. Percentage loss of tissue area *(PLA*, %) measured for tree and seedling needles of *Pinus pinaster* after dehydration. The reduction of the entire needle area ($PLA_{\text{Whole needle}}$) and individual tissue shrinkage for the needle epidermis, mesophyll, transfusion tissue, and vascular bundles were based on HRCT images, comparing needles at high water potential (P_{initial} = -0.4 and -0.1 MPa for tree and seedling needles, respectively) and low water potential (P_{final}= -8.4 and -7MPa for tree and seedling needles, respectively).

	$PLA_{\text{Whole needle}}$	$PLA_{\text{Epidermis}}$	$PLA_{\text{Mesophyll}}$	$PLA_{\text{Transfusion tissue}}$	$PLA_{\text{Vascular bundles}}$
Tree needle	23.7 %	5.4 %	15.4 %	46.9 %	2.5 %
Seedling needle	68.9 %	36.5 %	74.3 %	81.9 %	28.1 %

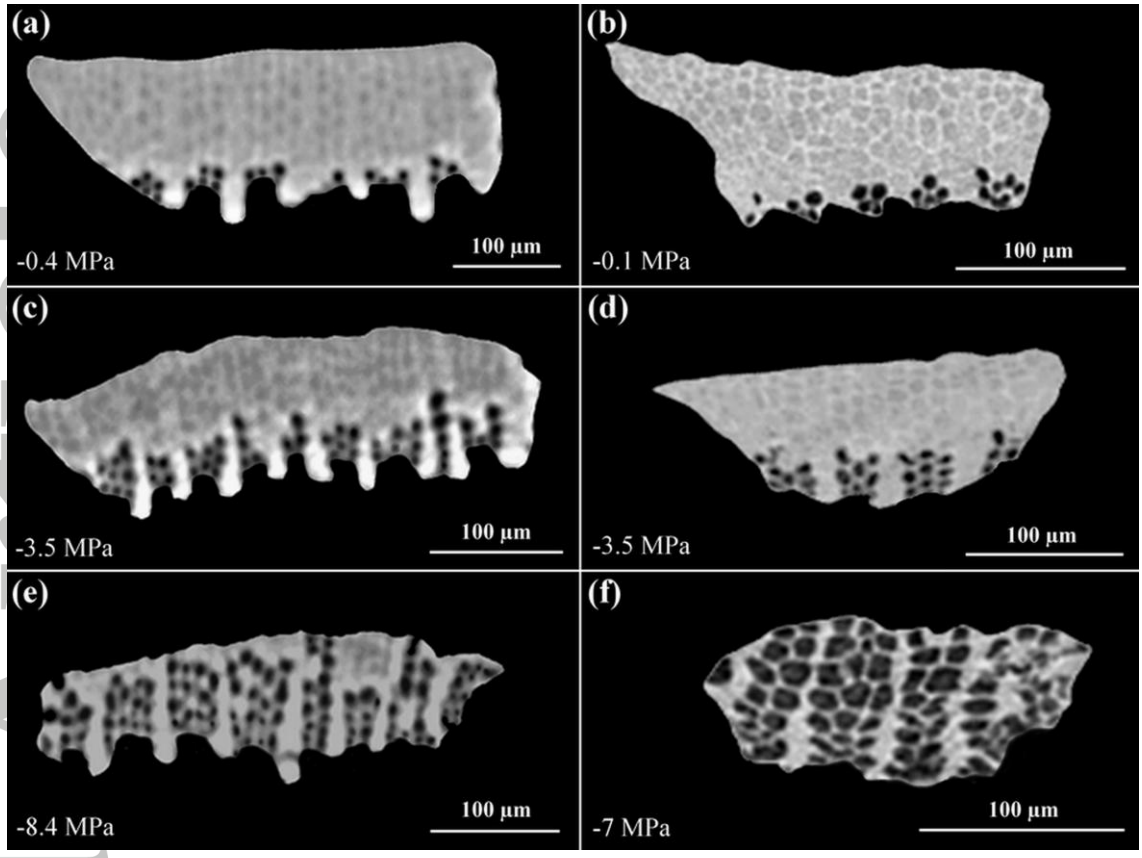

Figure 1. Transverse slices of *Pinus pinaster* needles from trees **(a, c, e, g)** and seedlings **(b, d, f)** based on X-ray computed tomography, showing details of the xylem tissue at different water potentials. The functional, water filled tracheids (grey) can be clearly distinguished from embolised (black) tracheids. The corresponding water potential (MPa) for each image is shown in the bottom left corner.

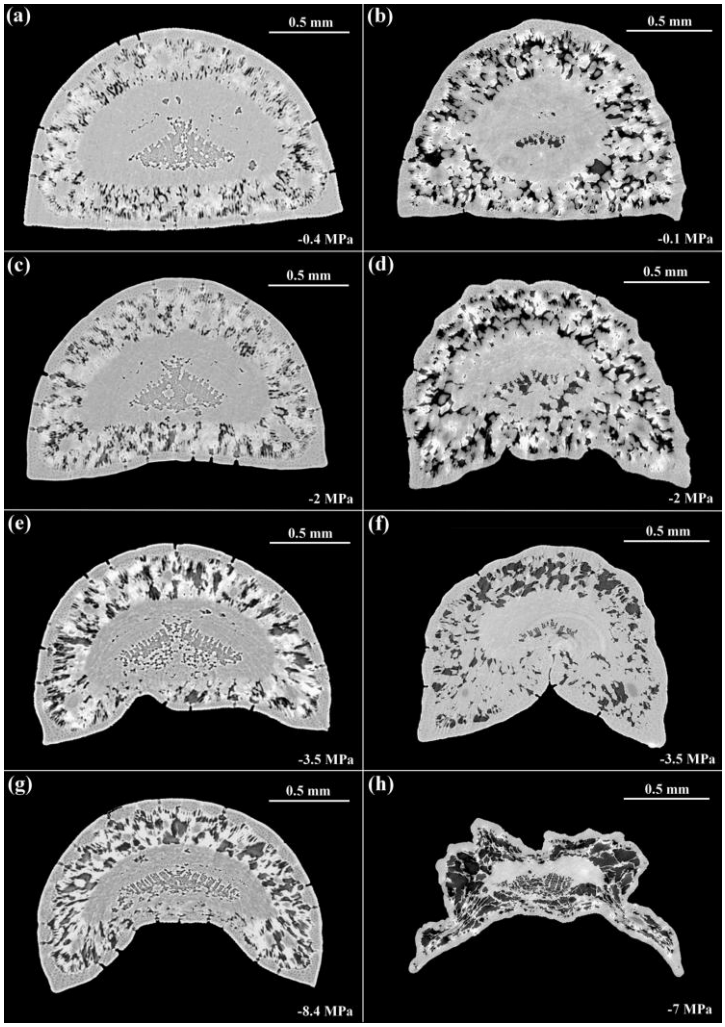

Figure 2. Transverse slices of *Pinus pinaster* needles based on X-ray computed tomography. The needles were from trees **(a, c, e, g)** and seedlings **(b, d, f, h)** at different xylem water potentials, showing shrinkage and morphological changes during dehydration. The corresponding water potential (MPa) for each image is shown in the bottom right corner.

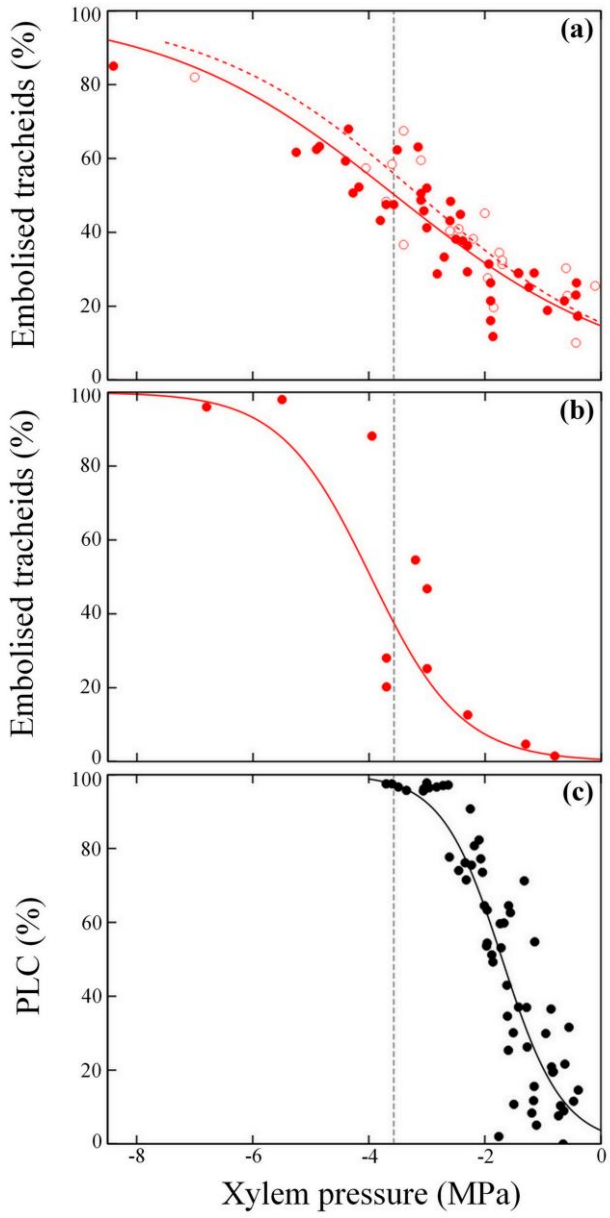

Figure 3. Vulnerability curves of *Pinus pinaster* needles (a and c) and stems (b) showing the percentage of embolised tracheids (a and b) and percentage loss of hydraulic conductance as a function of xylem pressure (MPa; c). **(a)** Needle vulnerability curves based on HRCT (red closed circles = needles from a 15-year old tree; red open circles = needles from 2-year-old seedlings). **(b)** Stem vulnerability curves based on HRCT (red circles), modified from Choat et al. (2015b). **(c)** Needle vulnerability curve based on the rehydration kinetic method (black closed circles). The vulnerability curves fitted are based on raw data. The vertical dashed lines correspond to 50% of embolised tracheids for the HRCT needle curves in (a).

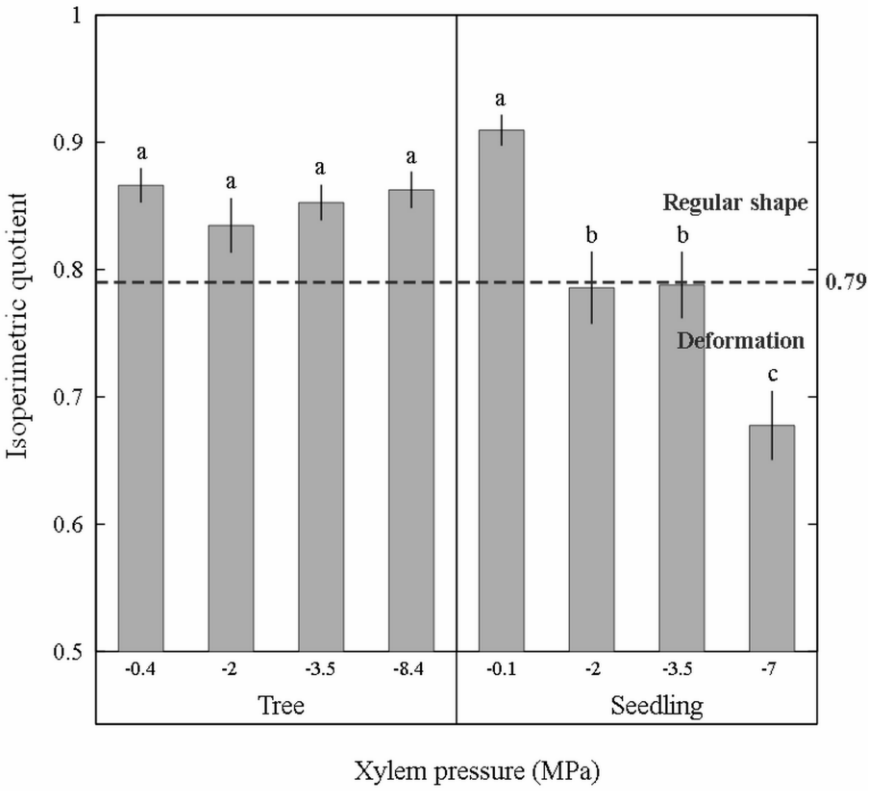

Figure 4. Variation in the isoperimetric quotient (*Q*) of xylem tracheids during dehydration of *Pinus pinaster* needles from trees and seedlings. *Q* equals 1 for a circular tracheid and decreases with tracheid deformation. When *Q* is below 0.79, the tracheid is considered to show deformation. Different letters indicate significant differences of *Q* with $p < 0.05$.

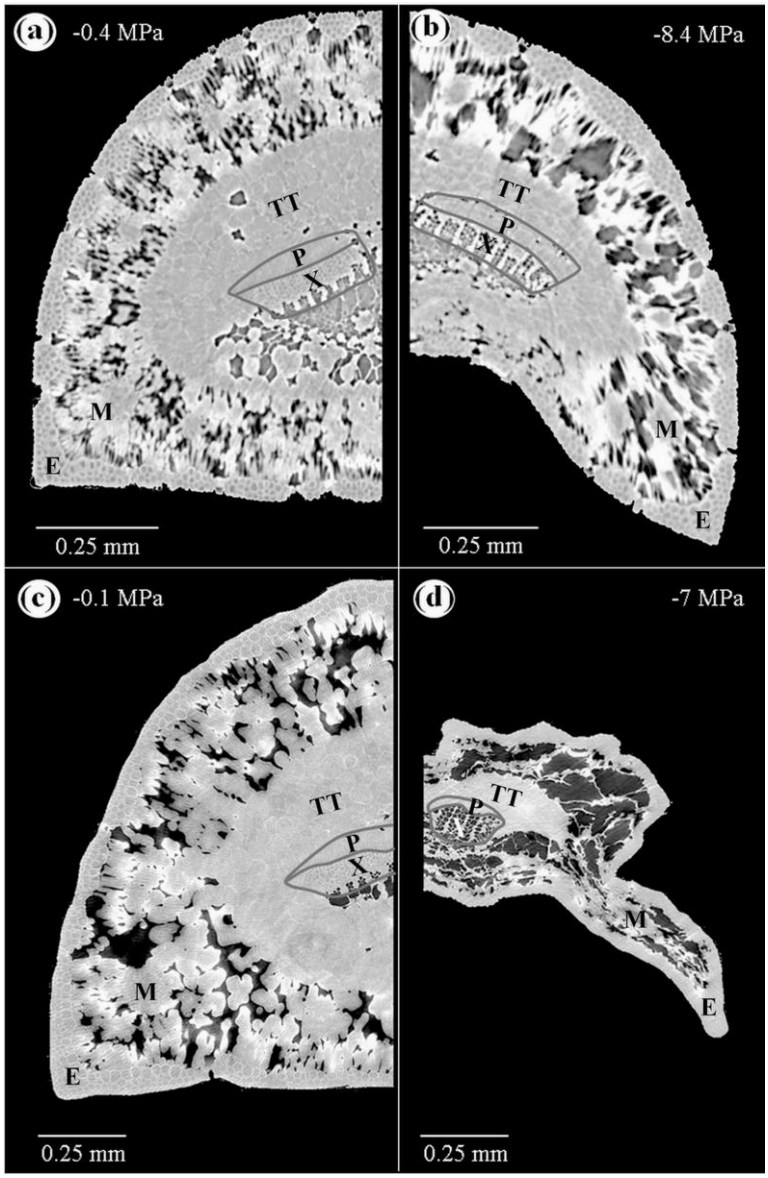

Figure 5. Transverse slices of *Pinus pinaster* needles based on X-ray computed tomography, showing micro-morphological differences between needles from a tree **(a, b)** and seedlings **(c, d)**, and between different levels of dehydration (a, c = well-watered; b, d = drought-stressed). The corresponding water potential (MPa) for each image is shown in the upper right corner. Anatomical details include the epidermis and hypodermis (E), mesophyll (M), transfusion tissue (TT), vascular bundles (grey inset), phloem (P) and xylem tissue (X). Both tree and seedling needles show strong deformation of their tissue under increasing drought stress due to shrinkage of mesophyll and transfusion tissue. Yet, a higher deformation is observed in the seedling needles than in tree needles. Contrary to xylem tracheids, no embolism is observed in transfusion tissue, but intracellular airspaces in the mesophyll cells enlarge with increasing dehydration.